

ZnO NANOPARTICLES: SURFACE AND X-RAY PROFILE ANALYSIS

M. A. ISMAIL^{a,c}, K. K. TAHA^{b,d,*}, A. MODWI^{a,b}, L. KHEZAMI^b

^a*Chemistry Department, College of Science & Technology, Omdurman Islamic University, Omdurman, Sudan*

^b*Department of Chemistry, College of Sciences, Al Imam Mohammad Ibn Saud Islamic University (IMSIU), Riyadh 11432, Saudi Arabia*

^c*College of Sciences and Arts, University of Shaqra, Sajir, Saudi Arabia*

^d*College of Applied and Industrial Sciences, University of Bahri, Khartoum, Sudan*

Herewith, we describe the synthesis of zinc oxide (ZnO) nanoparticles employing the precipitation approach and annealing it at various temperatures. The variations in the size and morphology of the nanostructures due to the temperature rise were probed by X-ray diffraction (XRD), Scanning Electron Microscopy (SEM), Energy Dispersive X-rays (EDX), BET Surface Analysis, Fourier Transformation Infrared (FTIR), and Thermogravimetric analysis (TG-DTA). The X-ray diffraction (XRD) graphs revealed a pure wurtzite structured ZnO nanoparticles. The Williamson–Hall X-ray peak profile analysis was employed to verify the crystallite sizes and lattice strain (ϵ) contributions to the broadening of the obtained nanoparticles XRD peaks. The data illustrated that the crystallite size calculated by Scherer's equation, Williamson–Hall models, and the particle size from SEM are positively correlated. The SEM images of the ZnO nanoparticles demonstrated semispherical shape that transformed to spherical aggregates with annealing temperature rise. BET Surface area analysis, confirmed the formation of a mesoporous ZnO with 25.3641 to 8.7781 m²/g surface area and 16.03 to 25.03 nm mean diameter as the temperature range was increased from 275°C to 600°C. Finally, the FTIR findings verified the ZnO formation as indicated by the existence of Zn-O stretching vibration at 443.96 cm⁻¹.

(Received July 9, 2018; Accepted October 12, 2018)

Keywords: Precipitation, ZnO nanoparticles, X-ray profile analysis, SEM; BET

1. Introduction

Recently, semiconductor nanomaterials have become a research focus owing to the attractive and fascinating optical and electrical properties, attributed to their size reduction, for diverse applications [1]. In particular, ZnO is a semiconductor nanostructure that has drawn substantial interest for applications such as sensing [2], bio-sensing [3], biological labels [4], dye-sensitized solar [5] and electrochemical cells [6]. In general, different approaches for ZnO nanomaterials synthesis such as chemical vapor deposition [7], spray pyrolysis [8,9], thermal decomposition [10], hydrothermal [11], sol-gel [12,13] and precipitation [14-16] have been adopted. Among these methods, low-temperature precipitation process is cost-effective and scalable for fabrication of a various forms of nano-structured ZnO. In prior works, the precipitation technique has been effectively employed to design different ZnO structures [17]. The characteristics of the ZnO nanoparticles greatly depend on the crystal size, morphology, surface area and porosity [11]. Several techniques for particle size measurement and morphology such as scanning electron microscopy (SEM) and transmission electron microscopy (TEM) analysis are employed. The XRD is suitable for determination of crystal structure, crystallite size and lattice parameters. The Williamson–Hall models are easy approach to calculate the crystallite size and lattice strain [18]. These two factors affect the Bragg's diffraction peaks in many ways and

* Corresponding author: kamalth60@gmail.com

consequently alter the peak's width and intensity along with reallocating the 2θ peak values accordingly [19,20].

This work considers with the formation of ZnO nanoparticles via a precipitation route by reacting a zinc precursor i.e. zinc nitrate hexahydrate $\text{Zn}(\text{NO}_3)_2 \cdot 6\text{H}_2\text{O}$ and sodium carbonate Na_2CO_3 in aqueous medium. The impact of annealing the obtained xerogel at 275°C , 375°C , 475°C and 600°C on the morphology and structure of ZnO nanoparticles were discussed based on the data achieved by various techniques. The XRD graphs of the fabricated nanostructures were explored by Scherer equation and Williamson Hall models to derive and compare the crystallites structural parameters i.e. the crystallite size, strain, stress and energy density. Moreover, the effect of strain insertion in the different models on the average size and anisotropic nature of the ZnO nanoparticles was examined.

2. Experimental procedure

2.1. Synthesis of ZnO nanoparticles

Zinc nitrate hexahydrate ($\text{Zn}(\text{NO}_3)_2 \cdot 6\text{H}_2\text{O}$), sodium carbonate (Na_2CO_3), absolute ethanol ($\text{CH}_3\text{CH}_2\text{OH}$, purity 99.7%), procured from Merck, and distilled-water were utilized in the research. All chemical were of analytical grade and used as received. A solution of (0.1 mole $\text{Zn}(\text{NO}_3)_2 \cdot 6\text{H}_2\text{O}$) was prepared by dissolving (29.747 g) in 200 ml of distilled water and 0.12 mole of Na_2CO_3 prepared by dissolving (12.7188 g) of Na_2CO_3 in 240 ml of distilled water. The prepared zinc nitrate solution was added to the other solution drop-wise under vigorous stirring. The white precipitate was separated by filtration then rinsed repeatedly with distilled water and ethanol, respectively and finally oven-dried at 110°C for 6 h to get the ZnO precursors. Annealing of the precursors was carried out in a muffle furnace at 275°C , 375°C , 475°C and 600°C for 4.0 h to acquire the ZnO nanostructures.

2.2 ZnO nanoparticles Characterization

The X-ray peak profile analysis (XPPA) was utilized to obtain the crystallite size, lattice parameters, lattice strain, lattice stress and strain energy density [18] using D8 Advance diffractometer (Bruker, Germany) with $\text{Cu-K}\alpha$ radiation ($\lambda = 0.15406 \text{ nm}$) with an accelerating voltage of 40 kV and an emission current of 30 mA. The morphology of the nanoparticles and its modification by temperature was done by scanning electron microscopy (SEM) (Phenom XL, Netherland). The elemental constituent of the prepared samples was studied by means of energy dispersive X-ray (EDX) analysis. Similarly, the alterations in surface area and porosity due annealing temperature were scrutinized via nitrogen adsorption analysis (BET) on a Micrometrics ASAP 2020 apparatus, (before doing the measurements the samples were degassed at 200°C for 20 min under 0 to 950 mmHg pressure). The thermal stability of the xerogel was examined through thermal gravimetric analysis TGA (Model: Mettler Toledo) under 0.02 to 250 K/min heating pace from ambient temperature till 1000°C in 150 μL crucible). The FTIR analysis was conducted to indicate the ZnO nanoparticles formation spectroscopy (Model: Nicolet 6700) in the range $4000 - 400 \text{ cm}^{-1}$ with a resolution of 4 cm^{-1}).

3. Results and discussion

3.1. The XRD analysis

3.1.1 Variation of crystalline size with annealing temperature

The XRD graphs of the ZnO samples illustrated in Fig. 1 exhibit a wurtzite (hexagonal phase) structure. The entire XRD peaks are in excellent conformity with the (JCPDS) card No. 36-1451 [21]. All examined samples have their strongest line corresponding to the (1 0 1) plane. In addition, as the annealing temperatures were increased the diffraction peaks became narrow with higher intensity. This is an indication of a good crystalline structure formation. Moreover, the broadening of the (101) diffraction peaks in Fig. 1 reflects the nano-sizes of the prepared ZnO

nanoparticles (Table 1) as previously reported [22]. Therefore, it is clear that there is an improved nanoparticles crystallinity with raising the temperature from 275^oC to 600^oC to provide adequate thermal energy [23]. The average crystallite sizes (D) of the nanostructures were computed by Debye Scherer expression [24]:

$$D = \frac{0.9\lambda}{\beta \cos \theta} \quad (1)$$

where λ 1.5406 Å is the Cu K α line, θ is the Bragg's XRD diffraction angle and β is the full width at half maximum (FWHM) in radians.

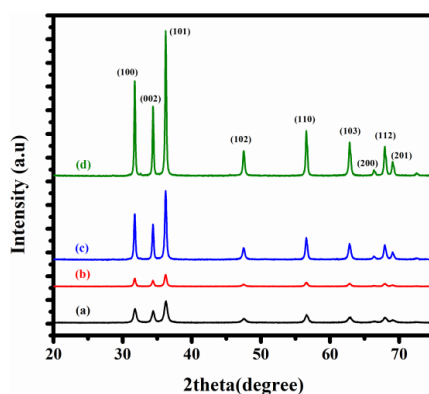


Fig. 1. XRD graphs of ZnO nanoparticles annealed at (a) 275^oC, (b) 375^o C, (c) 475^o C and (d) 600^oC.

Table 1. ZnO crystallite size at different annealing temperatures.

Annealing T °C	β radian	$X = 2\theta$	θ (degree)	Crystallite size (nm)
275	0.4342	36.2618	18.13091	19.25
375	0.3044	36.2216	18.11084	27.45
475	0.2446	36.2307	18.11535	34.18
600	0.2242	36.2267	18.11336	37.27

The lattice parameters (a and c) for ZnO nanoparticles were calculated using equation (2). The plane d-spacing (d) associated with the lattice parameters a , c and the Miller indices (h , k , l) is calculated via the theoretical (3) and Bragg's equations (4) as well [25-27]:

$$a = \frac{\lambda}{\sqrt{3} \sin \theta_{100}} \text{ and } c = \frac{\lambda}{\sin \theta_{002}} \quad (2)$$

$$\frac{1}{d^2} = \left[\frac{h^2 + hk + k^2}{a^2} \right] + \frac{l^2}{c^2} \quad (3)$$

$$d = \frac{\lambda}{2 \sin \theta} \quad (4)$$

where θ_{100} and θ_{002} are the diffraction peaks angles of the (100) and (002) planes respectively. The lattice parameters (a and c) (Table 2) are almost identical to those reported in the (JCPDS 36-

1451) card for ZnO [21]. The d-spacing values obtained from the Bragg's law (4), and the theoretical (3) equations, are almost identical (Table 2).

Table 2. ZnO samples Lattice parameters (c , a), and the inter-planer d -spacing.

Annealing T °C	2θ (degree)	Lattice parameters (\AA^0)		c/a	d (Bragg)	d (theoretical)
		(c)	(a)			
275	36.2618	5.2062	3.2479	1.6029	2.4753	2.4776
375	36.2216	5.2098	3.2510	1.6025	2.4776	2.4776
475	36.2307	5.2108	3.2519	1.6023	2.4772	2.4768
600	36.2267	5.2098	3.2509	1.6026	2.4198	2.4776
JCPDS 36-1451	36.2530	5.2070	3.2500	1.6021	-	-

The length of the Zn–O bond was calculated using equation (5)

$$L = \sqrt{\left[\left(\frac{a^2}{3}\right) + (0.5 - \mu)^2 * c^2\right]} \quad (5)$$

Where (μ) is the positional parameter of the wurtzite structure that indicates the extent of atoms displacement relative to the following plane in the c axis, as expressed with equation (6):

$$\mu = \frac{a^2}{3c^2} + 0.25 \quad (6)$$

The calculated ZnO bond length values (Table 3) are in excellent agreement with the 1.9767 \AA^0 reported in literature [28,29].

Table 3. Zn-O bond lengths of ZnO nanoparticles at different annealing temperatures.

Annealing T °C	$hkl(1\ 0\ 1)$			μ	L (\AA^0)
	2θ (degree)	c (\AA^0)	a (\AA^0)		
275	36.2618	5.2062	3.2479	0.3797	1.9770
375	36.2216	5.2098	3.2510	0.3798	1.9786
475	36.2307	5.2108	3.2519	0.3798	1.9792
600	36.2267	5.2098	3.2509	0.3797	1.9788

3.1.2. Williamson–Hall (W–H) methods for estimation of microstrain (ϵ) and crystallite size (D)

3.1.2.1. Uniform deformation model (UDM)

As stated by Williamson–Hall approach [30], strain and crystallite size have significant contribution to the broadening of diffraction lines (equation 7) [26,31]. One of Williamson–Hall equations is the uniform deformation model (UDM). In this model, it is presumed that a crystal is isotropic [18] and consequently its properties are unconnected with the crystallographic direction along which the measurement is done.

$$\beta_{\square kl} \cos \theta_{\square kl} = \frac{k\lambda}{D} + 4\varepsilon \sin \theta_{\square kl} \quad (7)$$

A plot of $\beta_{\square kl} \cos \theta_{\square kl}$ versus $4 \sin \theta_{\square kl}$ is a linear presentation of the data [18], the crystallite size (D) and microstrain (ε) are respectively obtained from the intercept and slope of the line (Figures. 2a, 2b, 2c and 2d). The results obtained are listed in Table 4.

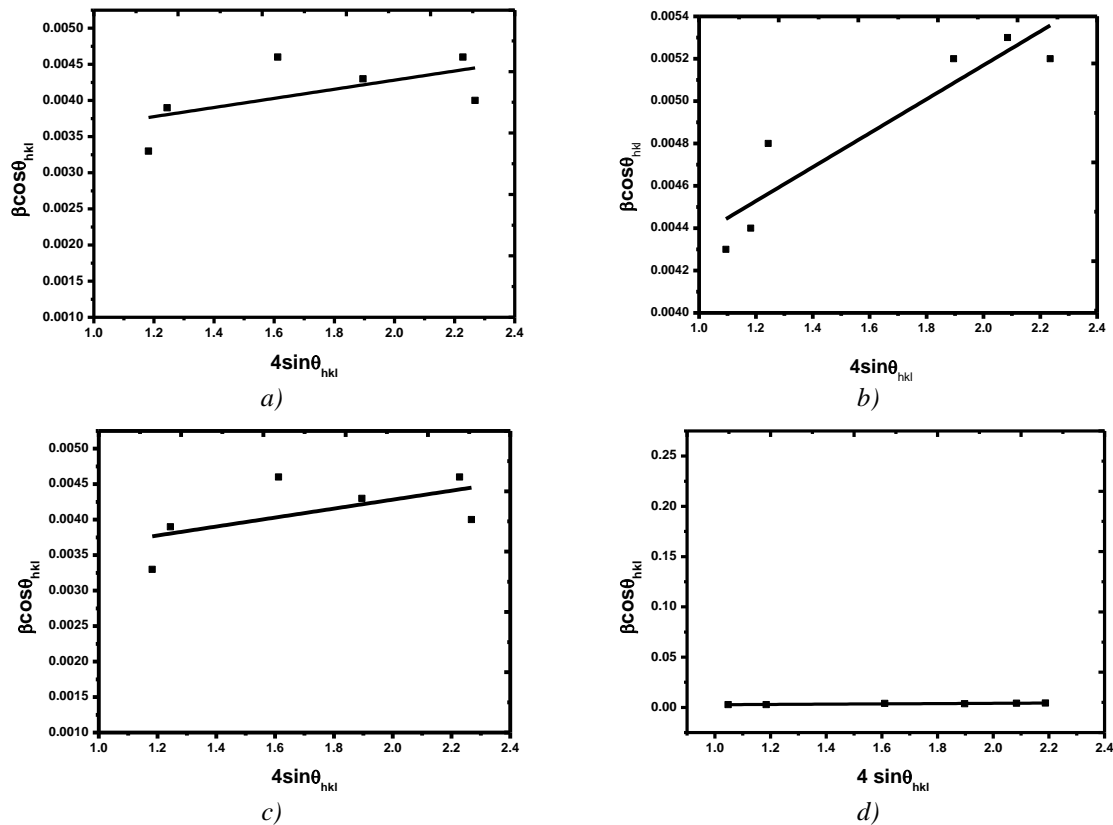


Fig. 2 UDM graph for the ZnO sample annealed at a) 275 °C; b) 375 °C; c) 475 °C; d) 600 °C.

3.1.2.2. Uniform stress deformation model (USDM)

As the isotropy and homogeneity conjecture is unfulfilled in many cases, a more realistic anisotropic model is therefore delegated. Accordingly, Williamson–Hall formula is modified by introducing an anisotropy term of strain (ε) [32]. In the Uniform stress deformation model (USDM), Hooke's law represents the strain in addition to a direct correlation linking the stress (σ), anisotropic microstrain (ε) and Young's modulus (Y_{hkl}) as given by $\sigma = \varepsilon Y_{hkl}$. For hexagonal ZnO nanoparticles (Y_{hkl}) was given as 127 GPa [26]. Thus, the Williamson–Hall expression is remodeled to (8):

$$\beta_{\square kl} \cos \theta_{\square kl} = \frac{k\lambda}{D} + \frac{4\sigma \sin \theta_{\square kl}}{Y_{\square kl}} \quad (8)$$

By plotting $\beta_{\square kl} \cos \theta_{\square kl}$ as a function of $\frac{4\sigma \sin \theta_{\square kl}}{Y_{\square kl}}$ the σ and D are determined from the slope and intercept respectively, while ε is enumerated applying Young's modulus, Y_{hkl} , of ZnO nanoparticles hexagon. Figures (3a, 3b, 3c and 3d) show the USDM for the four annealed samples and the data obtained is recorded Table 4.

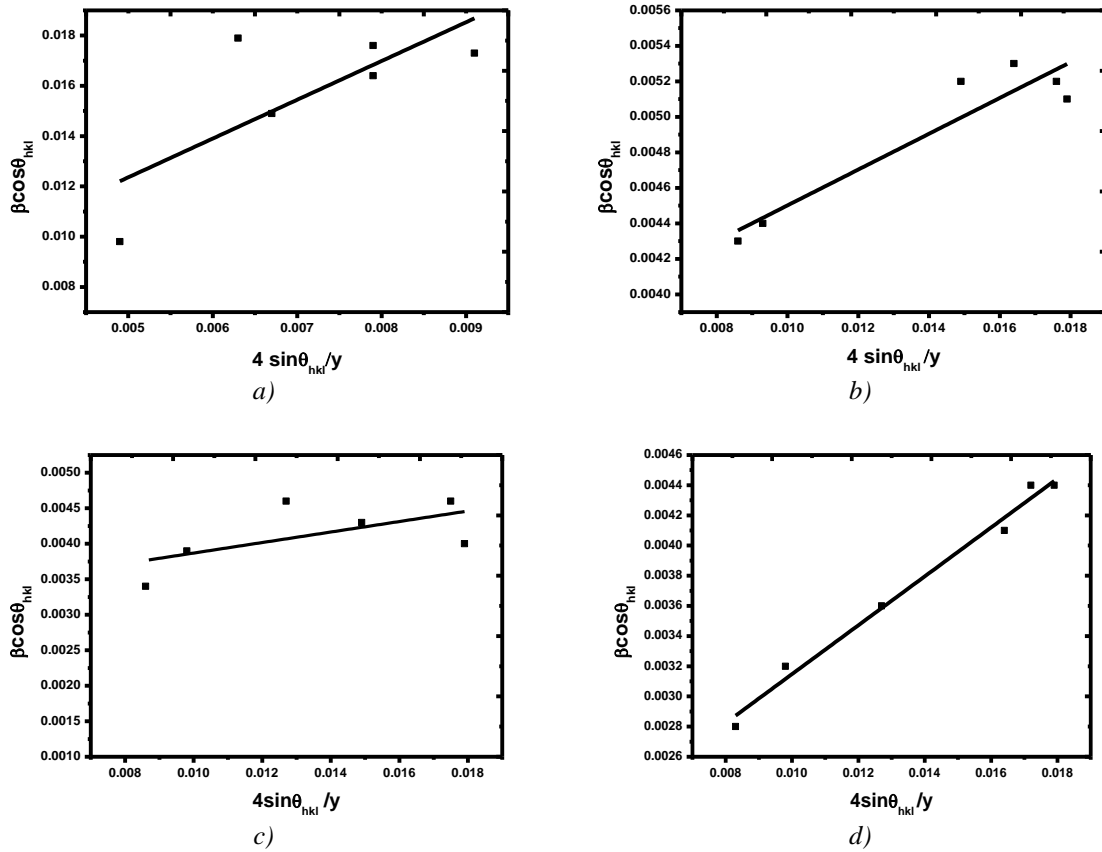


Fig. 3 UEDM for ZnO sample annealed at (a) 275 °C; b) 375 °C; c) 475 °C; d) 600 °C

3.1.2.3. Uniform deformation energy density model (UEDM)

Another form of Williamson–Hall methods termed the uniform deformation energy density model (UEDM) which is applied to deduce the crystal's energy density (u_{ed}). In case of elastic systems that comply with Hooke's law, u_{ed} is related to the strain by the formula $u_{ed} = (\epsilon^2 Y_{hkl})/2$ [26]. Equation (9) gives the UEDM term:

$$\beta_{\square kl} \cos \theta_{\square kl} = \left(\frac{k\lambda}{D}\right) + \left(4 \sin \theta_{\square kl} \left(\frac{2u_{ed}}{Y_{\square kl}}\right)^{0.5}\right) \quad (9)$$

$$\text{Where } \left(\frac{2u_{ed}}{Y_{\square kl}}\right)^{0.5} = 0.1255$$

After Plotting $\beta_{\square kl} \cos \theta_{\square kl}$ versus $4 \sin \theta_{\square kl} \left(\frac{2u_{ed}}{Y_{\square kl}}\right)^{0.5}$, we can use the slope to estimate the anisotropic energy density (u_{ed}). The stress (σ) and microstrain (ϵ) are calculated from (u_{ed}) and Y_{hkl} , while the crystallite size (D) is estimated from intercept [26]. Figures (4a, 4b, 4c and 4d) illustrate the UEDM for the four annealed samples and the results obtained are listed in Table 4.

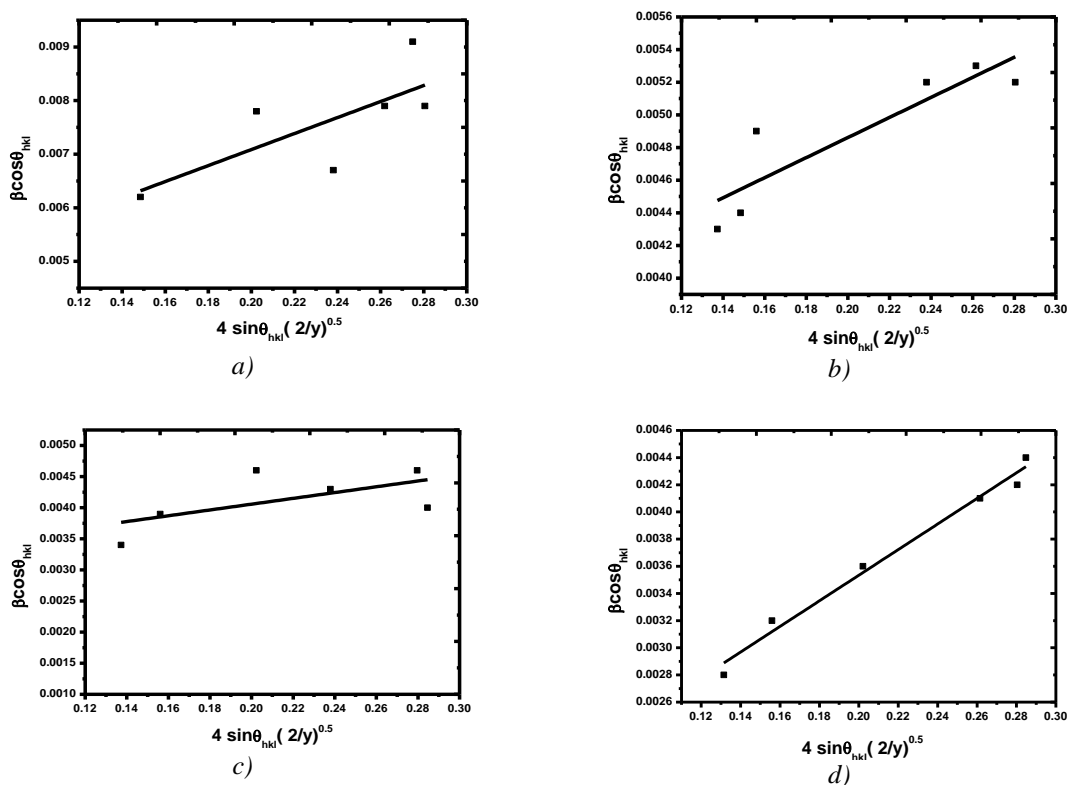


Fig. 4 UDEDM for the ZnO sample at a) 275°C; b) 375°C; c) 475°C; d) 600°C.

The mean crystallite size values applying the *UDM*, *UDSM*, and *UDEDM* models are virtually identical, indicating that the insertion of strain in the different formulae of W–H method has insignificant impact on the average (*D*) value. Nevertheless, the average crystallite sizes calculated from Scherrer's and W–H equations show little disparity that can be attributed to dissimilarity of particle size distribution averaging [30]. Though the data shows tremendously large crystallite size by all Williamson- Hall models for the sample annealed at 600°C, still our finding agree with previous investigations [33] that reported a convergence in the crystallite size results up to 450°C. All the ϵ and σ values obtained employing all the Williamson Hall models change inversely with the crystallite size in agreement with previously reported data [34,35]. When matching up the data obtained by the three models, it can be observed that there is great likeness in the parameters values confirming the isotropic character of the nanoparticle.

3.2. Change of ZnO morphology with annealing temperature:

3.2.1. Scanning Electron Microscopy (SEM)

Fig. 5 (a – e) portrays the (SEM) images of the precursor and ZnO nanoparticles after annealing. The micrographs reveal ZnO nanoparticles with particle like morphological appearance and spherical shape with homogeneous size distribution, as described in literature [27]. It is clear that nanoparticles get severely aggregated with the increasing of temperature leading to larger particle size formation Table 4. This agglomeration and clustering of nanoparticles is an obvious result of their high surface energy [28]. The nanoparticles diameter obtained from scanning electron microscopy (SEM) is greater than the crystallite size from Scherer and W–H calculations. This reveals the polycrystalline nature of the nanoparticles that enclose quite a lot of ~36 nm crystallite grains [36]. In view of the fact that these polycrystalline particles experience stress evaluation of their dislocations density (ρ) is estimated by inserting the crystallite grain size (*D*) in

the equation [31,37] $\rho = \left(\frac{1}{D^2}\right)$. Therefore a dislocation density of $7.72 \times 10^{-4} \text{ nm}^{-2}$ is evidenced for the ZnO nanoparticles synthesized in this work.

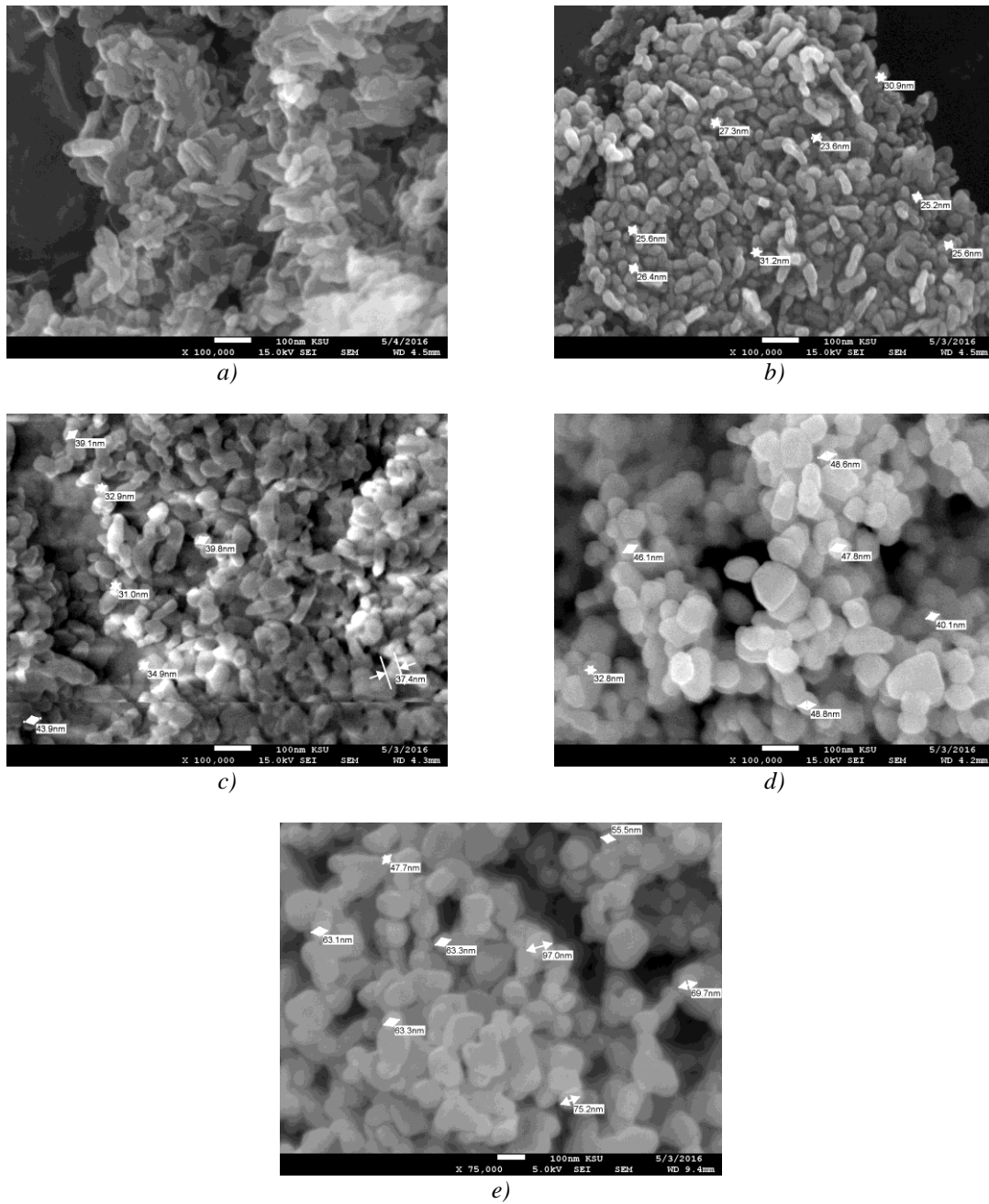


Fig. 5. SEM of ZnO Xerogel at a) as deposited; b) at 275 °C; c) 375 °C; d) 475 °C; e) 600 °C

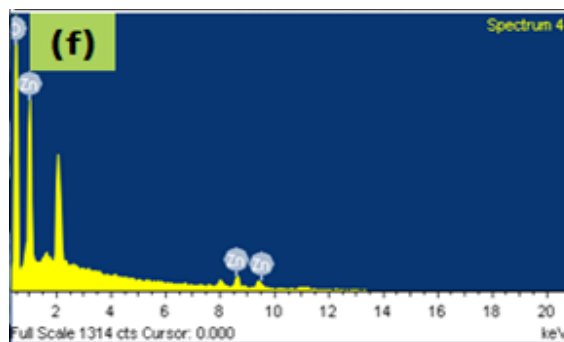


Fig. 5f. EDS of ZnO nanoparticles

Table 4. Particle size from SEM results and crystallite size calculated using Scherrer and Williamson- Hall models.

Annealing T °C	SEM (nm)	Scherrer D (nm)	Williamson- Hall method								
			UDM			USDM			UEDM		
			D (nm)	ϵ 10^{-4}	χ	D (nm)	ϵ $\times 10^{-4}$	σ (MPa)	D (nm)	ϵ $\times 10^{-4}$	σ (MPa)
275	26.97	19.25	34.65	24.0	30.7	15	185.64	30.8	95	172.2	0.0117
375	37.00	27.45	33.39	4.0	32.8	4	46.6	32.6	48	86.12	0.0029
475	50.33	34.18	46.35	3.5	39.04	2	20.8	39.26	33	59.20	0.00138
600	100.48	37.27	167.7	2.0	96.25	13	16.3	95.58	19	40.88	0.0102

3.2.2. Energy dispersive analysis x- ray (EDS) spectra:

The EDS study (Fig.5f as a representative) reveals that Zn and O are the major constituents of the prepared material and the weight percentages of elemental constituents of the samples can be seen in Table. 5. Obviously the carbon ratio diminishes due to the annealing temperature elevation.

Table 5.Elemental composition of ZnO precursor and annealed samples from EDS.

Annealing T °C	The elements (%)		
	C K	O K	Zn L
ZnO Precursor	24.62	29.89	45.49
275	13.24	18.66	68.10
375	11.40	16.91	71.69
475	12.95	12.96	68.28
600	3.26	15.65	81.10

3.3. BET Surface area analysis of the as- obtained ZnO precursor and ZnO nanoparticles

The specific surface area (S_{BET}), pore volume and average diameter (BJH) of the as-obtained ZnO precursor and the four ZnO samples annealed at 275°C, 375°C, 475°C and 600°C were determined by N_2 adsorption. Fig. 6 displays the N_2 adsorption-desorption isotherms of ZnO precursor and ZnO samples annealed at different temperatures. The graph (Fig. 6) display a Type-IV isotherm given by the IUPAC classification [38]. The isotherm indicates that the micropores are filled with the gas at extremely low pressure then a monolayer starts to form at the knee,

whereas a multilayer is formed as the press reaches a medium value. Finally capillary condensation prevails as the pressure gets higher. Fig. 6 shows that the samples give rise to H3 hysteresis as an indication of having slit-shaped pores beside that the isotherms of type H3 do not illustrate any limiting adsorption at high P/P^0 which is a sign of particles aggregation in consistence with obtained SEM results.

Fig. 7 portrays the Barret-Joyner-Halenda (BJH) pore size distribution for all specimens. All sizes are in the mesoporous range, which coincides with type-IV adsorption isotherm. The Average of pores diameter (Fig. 7) are less than 50 nm, which is consistent with mesoporous material characteristics. Table 6 demonstrates a notable diminish in the surface area of ZnO samples from 25.3641 to 8.7781 m^2/g and pore volume from 0.3536 to 0.0270 cm^3/g as the temperature was elevated to 600°C. The reduction in surface and pore volume as a result of annealing may be the collapse the pores and the consequent nanoparticles agglomeration that leads to a reduction in specific surface area and pore volumes [39]. The average diameter of the particles (d_{BET}) was calculated from the S_{BET} using the formula [40]:

$$d_{BET} = \frac{6000}{SSA(m^2/g)\rho(g/cm^3)} \quad (10)$$

Where SSA is the specific surface area and ρ is the material density. The d_{BET} values Table 6 are comparable with those obtained from the W-H models Table 4.

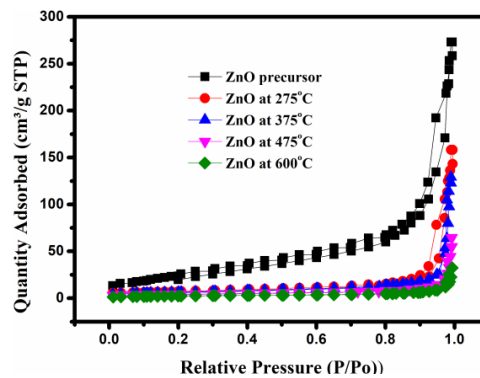


Fig. 6. Nitrogen adsorption-desorption isotherms of ZnO precursor and annealed ZnO nanoparticles.

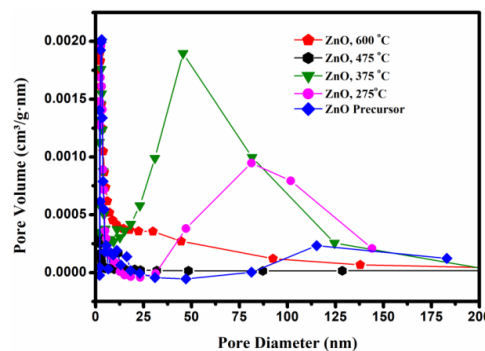


Fig. 7. Pore size distribution of ZnO precursor and annealed ZnO nanoparticles.

Table 6. BET analysis surface area and porosity of ZnO precursor and ZnO samples.

Annealing T °C	S _{BET} (m ² /g)	Pore volume (cm ³ /g)	Average pore width (nm)	BJH pore diameter (nm)	d _{BET} (nm)
ZnO precursor	87.43	0.3536	16.18 - 17.24	14.61 - 14.74	14.0
275	25.36	0.1936	30.53 - 31.39	41.83 - 37.04	42.0
375	22.81	0.1235	21.65 - 33.38	36.06- 34.83	46.9
475	15.16	0.0506	13.36 - 22.36	38.28 - 35.29	70.61
600	8.78	0.0270	12.32 - 17.79	23.93 -22.57	121.9

3.4. Thermogravimetric analysis of ZnO precursor (TG-DTA)

TG-DTA measurement was performed to study the thermal stability the ZnO precursor. As revealed by Fig. 8, there is a minor weight loss ($\approx 5\%$) at around 200°C owing to moisture and volatile solvent desorption. The major weight loss step in the $236^{\circ}\text{C} - 289^{\circ}\text{C}$ temperature range, is an indication of the precursor decomposition and the loss of CO_2 [16]. The rapid weight loss and the endothermic peak around 236°C to 289°C may be attributed to decomposition of the precursor, and the thermal decomposition was almost completed before 300°C was attained. This implies that 300°C would be a satisfactory temperature for the precursor decomposition and acquiring the ZnO nanoparticles.

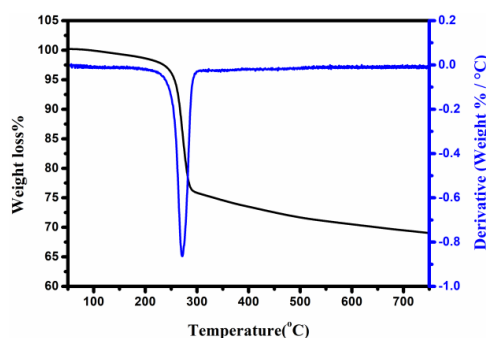


Fig. 8. TG-DTA graphs of the ZnO precursor.

3.4. Fourier transforms infrared studies (FTIR) ZnO at 275°C

FTIR spectra were recorded for ZnO annealed at 275°C in the range of $4000 - 400\text{ cm}^{-1}$. The obtained spectra are presented in Fig. 9. The appearance of absorption peaks around 3442.25 cm^{-1} and 1622.22 cm^{-1} can be ascribed to O-H stretching and bending vibrations, respectively. The $\text{O} = \text{C} = \text{O}$ vibration of CO_2 molecule existing in air [41] is indicated by band around 2427.75 cm^{-1} . The presence of nitrate peaks at around 836.35 cm^{-1} can be originated from zinc nitrate used as zinc source. The formation of the target ZnO nanoparticles is confirmed by the IR broad absorption feature positioned at 443.96 cm^{-1} which agrees with the stretching vibration of Zn-O [42].

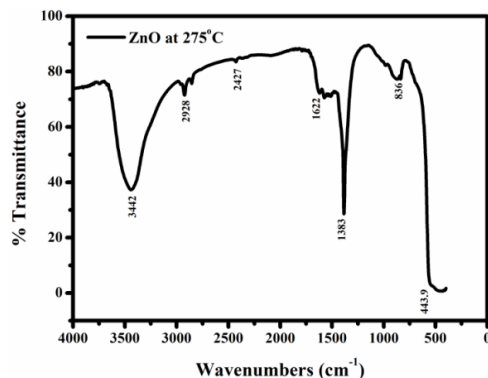


Fig.9. FT-IR spectra of ZnO annealed at 275°C.

4. Conclusions

This paper describes the production of ZnO nanoparticles via the precipitation method using zinc nitrate hexahydrate $\text{Zn}(\text{NO}_3)_2 \cdot 6\text{H}_2\text{O}$ and sodium carbonate Na_2CO_3 and a subsequent annealing of the resulting nanostructures at 275°C to 600°C temperature range. TGA-DTA measurements revealed the decomposition of the precursor to form ZnO particles above 289°C. The XRD data affirmed the formation of ZnO nanoparticles having the characteristic wurtzite (hexagonal phase) structure.

The broadening of the XRD peaks analysis by both Scherrer's and W–H formulae denoted an increment in ZnO nanoparticles average crystallite size with the rise in temperature. However, there was a small variation between ZnO crystallite size enumerated from XRD data and those obtained from SEM which can be attributed to agglomeration in products. The values of the strain, stress, and energy density estimated using the W–H models were comparable with good concurrence between them. BET results reveal a Type-IV isotherm with H3 hysteresis and a mesoporous pore size distribution for all samples. The FTIR results substantiated the synthesis of ZnO nanoparticles as stipulated by a peak at 443.96 cm^{-1} ascribed to the Zn-O bond.

References

- [1] M. Li, et al., *Materials Letters* **61**, 690 (2007).
- [2] J. Huang, et al., *Sensors and Actuators B: Chemical* **146**, 206 (2010).
- [3] C.Xia, N.Wang, L.Lidong, G. Lin, *Sensors and Actuators B: Chemical* **129**, 268 (2008).
- [4] M.Bruchez, M.Moronne, P.Gin, S. Weiss, A. P.Alivisatos, *Science* **281**, 2013 (1998).
- [5] D.Lee, et al., *Solar Energy Materials and Solar Cells* **95**, 365 (2011).
- [6] H.Weller, *Advanced Materials* **5**, 88 (1993).
- [7] E.Muccillo, S.Tadokoro, R. Muccillo, *Journal of Nanoparticle Research* **6**, 301 (2004).
- [8] W.Yu, X.Li, X.Gao, *Crystal Growth & Design* **5**, 151 (2005).
- [9] T.-Q.Liu, O.Sakurai, N.Mizutani, M. Kato, *Journal of Materials Science* **21**, 3698 (1986).
- [10] C.Liewhiran, S.Seraphin, S.Phanichphant, *Current Applied Physics* **6**, 499 (2006).
- [11] B.Liu, H. C. Zeng, *Journal of the American Chemical Society* **125**, 4430 (2003).
- [12] R. J.Lauf, W. Bond, *Am. Ceram. Soc. Bull.:(United States)* **63** (1984).
- [13] W.Peng, S. Qu, G.Cong, Z.Wang, *Materials Science in Semiconductor Processing* **9**, 156 (2006).
- [14] C.Chen, P.Liu, C.Lu, *Chemical Engineering Journal* **144**, 509 (2008).
- [15] C.Li, et al., *Journal of Alloys and Compounds* **475**, 718 (2009).
- [16] Z.Siqingaowa, H.Yao, *Frontiers of Chemistry in China* **1**, 277 (2006).
- [17] S.Sepulveda-Guzman, et al., *Materials Chemistry and Physics* **115**, 172 (2009).
- [18] T.Ungár, *Journal of Materials Science* **42**, 1584 (2007).

- [19] B. D.Cullity, J. W.Weymouth, *American Journal of Physics* **25**, 394 (1957).
- [20] C.Suryanarayana, M. G.Norton, (Springer Science & Business Media, 2013).
- [21] F. H.Chung, *Journal of Applied Crystallography* **7**, 519 (1974).
- [22] B. D.Cullity, S. R.Cullity, S.Stock, *Elements of X-ray Diffraction* (2001).
- [23] D.Raoufi, T.Raoufi, *Applied Surface Science* **255**, 5812 (2009).
- [24] C. S.Barrett, *Structure of metals* (McGraw-Hill Book Company, Inc.; New York, 1943).
- [25] U.Seetawan, et al., *Materials Sciences and Applications* **2**, 1302 (2011).
- [26] T.Pandiyarajan, B.Karthikeyan, *Journal of Nanoparticle Research* **14**, 647 (2012).
- [27] U. Pal, et al., *Optical Materials* **29**, 65 (2006).
- [28] A.Modwi, et al., *Journal of Ovonic Research* **12** (2016).
- [29] K.Taha, M. M'hamed, H.Idriss, *J. Ovonic Res* **11**, 271 (2015).
- [30] A. K.Zak, W. A.Majid, M. E.Abrishami, R.Yousefi, *Solid State Sciences* **13**, 251 (2011).
- [31] P.Bindu, S. Thomas, *Journal of Theoretical and Applied Physics* **8**, 123 (2014).
- [32] S.Brandstetter, P.Derlet, S. Van Petegem, H. Van Swygenhoven, *Acta Materialia* **56**, 165 (2008).
- [33] V.Mote, Y.Purushotham, B.Dole, *Journal of Theoretical and Applied Physics* **6**, 6 (2012).
- [34] R.Jacob, J. Isac, *Int. J. Chem. Studies* **2**, 12 (2015).
- [35] S.Amirkhanlou, M. Ketabchi, N. Parvin, *Materials Letters* **86**, 122 (2012).
- [36] S. G.Pandya, J. P.Corbett, W. M.adwisienczak, M. E.Kordesch, *Physica E: Low-dimensional Systems and Nanostructures* **79**, 98 (2016).
- [37] G.Ouyang, X. Li, X.Tan, G. Yang, *Applied Physics Letters* **89**, 031904 (2006).
- [38] S.Bahri, Omdurman, S. kinetic and thermodynamic studies of trivalent arsenic removal by indium-doped zinc oxide nanopowder.
- [39] R.Sivakami, S. Dhanuskodi, R. Karvembu, *Spectrochimica Acta Part A: Molecular and Biomolecular Spectroscopy* **152**, 43 (2016).
- [40] S. Kuśnieruk, et al., *Beilstein Journal of Nanotechnology* **7**, 1586 (2016).
- [41] L.Shi, S. Gunasekaran, *Nanoscale Research Letters* **3**, 491 (2008).
- [42] N.Kannadasan, et al., *Spectrochimica Acta Part A: Molecular and Biomolecular Spectroscopy* **143**, 179 (2015).